

Statistical Study of Network Jets Observed in the Solar Transition Region: a Comparison Between Coronal Holes and Quiet-Sun Regions

Nancy Narang¹ · Rebecca T. Arbacher^{2,3} · Hui Tian⁴ ·
Dipankar Banerjee^{1,5} · Steven R. Cranmer⁶ ·
Ed E. DeLuca² · Sean McKillop²

Received: 26 September 2015 / Accepted: 31 March 2016 / Published online: 18 April 2016
© Springer Science+Business Media Dordrecht 2016

Abstract Recent IRIS observations have revealed a prevalence of intermittent small-scale jets with apparent speeds of $80\text{--}250\text{ km s}^{-1}$, emanating from small-scale bright regions inside network boundaries of coronal holes. We find that these network jets appear not only in coronal holes but also in quiet-sun regions. Using IRIS 1330 Å (C II) slit-jaw images, we extracted several parameters of these network jets, *e.g.* apparent speed, length, lifetime, and increase in foot-point brightness. Using several observations, we find that some properties of the jets are very similar, but others are obviously different between the quiet Sun and coronal holes. For example, our study shows that the coronal-hole jets appear to be faster and longer than those in the quiet Sun. This can be directly attributed to a difference in the magnetic configuration of the two regions, with open magnetic field lines rooted in coronal holes and magnetic loops often present in the quiet Sun. We also detected compact bright loops that are most likely transition region loops and are mostly located in quiet-Sun regions. These small loop-like regions are generally devoid of network jets. In spite of different magnetic structures in the coronal hole and quiet Sun in the transition region, there appears to be no substantial difference for the increase in

Electronic supplementary material The online version of this article (doi:[10.1007/s11207-016-0886-1](https://doi.org/10.1007/s11207-016-0886-1)) contains supplementary material, which is available to authorized users.

✉ D. Banerjee
dipu@iiap.res.in
N. Narang
nancy@iiap.res.in
H. Tian
huitian@pku.edu.cn

¹ Indian Institute of Astrophysics, Koramangala 2nd Block, Bangalore 560034, India

² Harvard-Smithsonian Center for Astrophysics, Garden Street, Cambridge, UK

³ Department of Physics, Columbia University, Palisades, NY 10027, USA

⁴ School of Earth and Space Sciences, Peking University, Beijing, 100871, China

⁵ Center of Excellence in Space Sciences, IISER, Kolkata, India

⁶ Department of Astrophysical and Planetary Sciences, Laboratory of Atmospheric and Space Sciences, University of Colorado, Boulder, CO 80309, USA

footpoint brightness of the jets, which suggests that the generation mechanism of these network jets is very likely the same in both regions.

Keywords Chromosphere · Transition region · Coronal hole · Jets

1. Introduction

The solar chromosphere and transition region (TR) act as an interface between the relatively cool photosphere ($\sim 6 \times 10^3$ K) and the hot corona ($\sim 10^6$ K) and hence play a key role in the formation and acceleration of solar wind. Numerous investigations are being carried out to understand where the solar wind originates and how it is accelerated (for recent reviews see Cranmer, 2009 and Hansteen and Velli, 2012). Dark regions in coronal images indicate coronal holes (CHs), which are the commonly accepted large-scale source regions of the high-speed solar wind. On the other hand, the quiet-Sun (QS) regions (QS is a generic term for regions too bright to be coronal holes, but too dim to be regarded as magnetically active) are considered to be one possible large-scale source of the low-speed component of the solar wind (Habbal, Woo, and Arnaud, 2001; He, Tu, and Marsch, 2007; Tian *et al.*, 2011). However, identifying the precise origin sites of the two different components of the solar wind in the respective regions is still a challenging task because it requires high-resolution observations of the chromosphere and TR.

Coronal holes are regions of low-density plasma in the solar corona whose magnetic fields open freely into interplanetary space. The existence of coronal holes was first recognized in the late 1950s, when Waldmeier (1956) reported long-lived regions of negligible intensity in images made with a visible-light coronagraph. In coronal images, CHs appear darker than QS regions because they emit less in the ultraviolet and X-rays and are maintained at a lower temperature than the surrounding QS region. The different magnetic structures of CH and QS regions at coronal heights are responsible for their different appearance in coronal lines (Wiegelmann and Solanki, 2004; Tian *et al.*, 2008b). CHs are dominated by open magnetic field lines expanding super-radially in the heliosphere, whereas QS regions are dominated by closed magnetic loops of different sizes.

Although CHs emit significantly less at coronal temperatures than QS regions, in most of the chromospheric and lower TR lines they can hardly be distinguished. Typically, lines from ions formed around 10^4 K sample the chromosphere, which is characterized by a cell-like pattern of super-granular surface flows. The super-granular network is the same in CHs and QS regions. As the temperature increases past 10^5 K in the thin and chaotic TR, CHs become distinguishable as areas of lower density and temperature. In spectroscopic observations, line parameters in the two regions also differ only for TR and coronal lines. For instance, Wang *et al.* (2013) used spectroscopic observations of the *Solar Ultraviolet Measurements of Emitted Radiation* instrument (SUMER, Wilhelm *et al.*, 1995) onboard the *Solar and Heliospheric Observatory* (SOHO) spacecraft to investigate the Doppler shifts and nonthermal line widths of various lines spanning the solar atmosphere from the chromosphere to the TR. It was observed that most of the TR region lines in network regions are broader and more blueshifted in CH than in QS regions. On the other hand, no such distinction between CH and QS regions was observed for the chromospheric lines.

High-resolution observations from the *Interface Region Imaging Spectrograph* (IRIS: De Pontieu *et al.*, 2014b) have revealed unprecedented levels of details in the less studied solar TR, the layer between chromosphere and corona. Tian *et al.* (2014) recently reported the detection of prevalent small-scale high-speed jets with TR temperatures from

the network structures of CHs. These network jets can be significantly observed in slit-jaw images (SJIs) of the Mg II 2796 Å (10^4 K, chromosphere), C II 1330 Å (3×10^4 K, lower TR), and Si IV 1440 Å (8×10^4 K, TR) passbands of IRIS, although they are best visible in C II 1330 Å. They can also be identified in the clean spectra of Si IV lines. The most obvious signature of the network jets is the significant broadening of the line profiles. They originate from small-scale bright regions, often preceded by footpoint brightenings. Tian *et al.* (2014) concluded that the existence of network jets is consistent with the magnetic furnace model of the solar wind (Axford and McKenzie, 1992; Tu *et al.*, 2005; Yang *et al.*, 2013) and thus may serve as strong candidates for the supply of mass and energy to the solar wind and corona. Tian *et al.* (2014) also suggested that some of these network jets may be the on-disk counterparts and TR manifestations of the chromospheric type II spicules (see also Pereira *et al.*, 2014, De Pontieu *et al.*, 2014a, Rouppe van der Voort *et al.*, 2015, Skogsrud *et al.*, 2015).

The network jets in CHs, as reported in Tian *et al.* (2014), have widths of ≤ 300 km with lifetimes of 20–80 s and lengths of 4–10 Mm. The authors calculated apparent speeds of the jets, which are 80–250 km s⁻¹ in CHs. We observe that the network jets appear not only in CHs, but also in QS areas. In this article, we study comparatively various properties of these short-lived small-scale network jets in CH and QS regions using IRIS SJIs in the 1330 Å passband.

2. Data Analysis

2.1. Details of Observations

Four datasets obtained with IRIS are used in this article, two of which are of CH and two of QS regions. Details of the observations are showcased in Table 1. It is important to note that all four datasets are high-cadence sit-and-stare observations, which is essential for studying the dynamics of the short-lived jets. In Figure 1 the observed regions on the solar disk are shown as rectangles outlined in the coronal images taken in the 193 Å passband of the *Atmospheric Imaging Assembly* (AIA; Lemen *et al.*, 2012) onboard the *Solar Dynamics Observatory* (SDO). The calibrated level 2 data of IRIS were used in our study. Dark-current subtraction, flat-field correction, and geometrical correction have all been taken into account in level 2 data (De Pontieu *et al.*, 2014b). Tian *et al.* (2014) mentioned that the network jets are best visible in 1330 Å images. We therefore here used SJIs in only this passband (see Figure 2). The 1330 Å passband of IRIS samples emission from the strong C II 1334/1335 Å lines formed in the lower TR ($\sim 3 \times 10^4$ K), although, being a broad passband, it also includes UV continuum emission formed in the upper photosphere. For instance, the observed ubiquitous grain-like structures in SJIs probably originate from UV emission from granules (magneto-convective cells in the solar photosphere)

Table 1 Summary of sit-and-stare observations. For all the datasets mentioned here, the field of view is $119'' \times 119''$, the exposure time is 4 s, and the cadence is 10 s.

Dataset	Observation time	Target	Pointing (X, Y)
A	2014-01-23 08:48 to 09:39 UT	CH	$812'', 464''$
B	2014-01-24 09:11 to 10:06 UT	CH	$485'', 670''$
C	2014-01-29 01:23 to 02:21 UT	QS	$801'', 447''$
D	2014-02-12 10:04 to 10:46 UT	QS	$-781'', 582''$

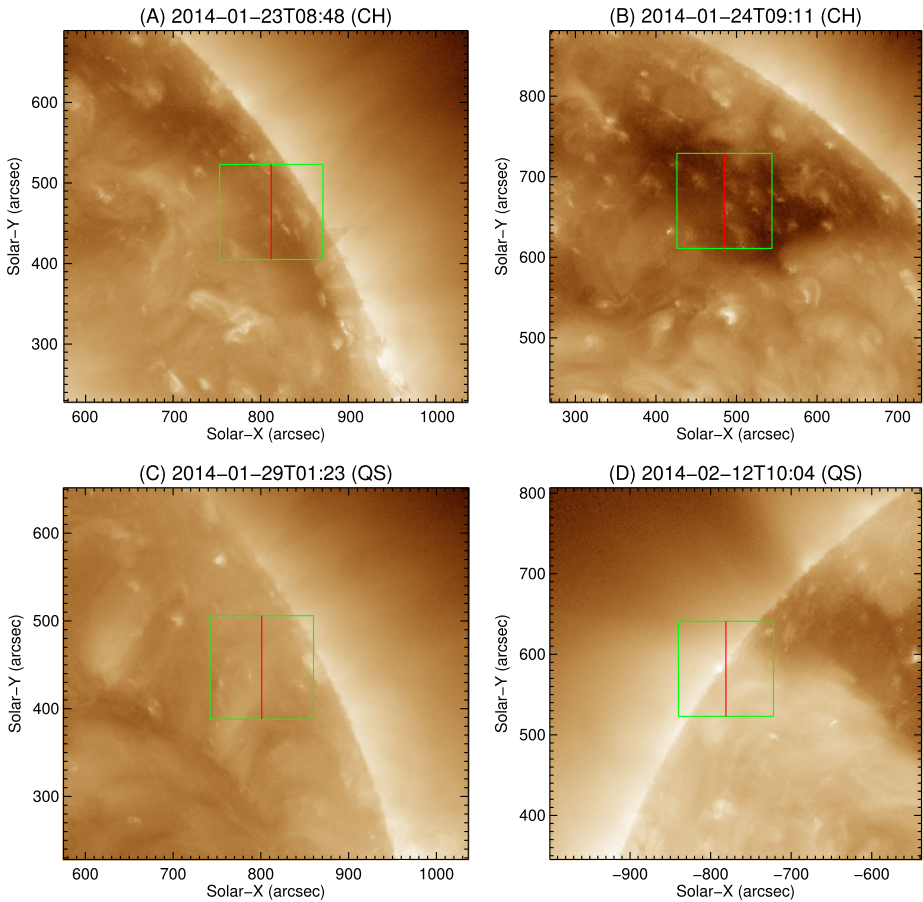


Figure 1 IRIS observation regions outlined in AIA 193 Å images. In each panel, the green rectangle outlines the field of view (FOV) of the IRIS SJIs and the red line shows the position of the slit. The details of the four observations shown here are provided in Table 1.

and acoustic or magneto-acoustic shocks (Carlsson and Stein, 1997, Rutten, De Pontieu, and Lites, 1999, Martínez-Sykora *et al.*, 2015, also see the supplementary materials of Tian *et al.*, 2014 for a detailed discussion). We explain in Section 2.3 that it is important to choose close-to-limb observations to minimize projection effects. Not many close-to-limb observations with a large field of view and high cadence in the 1330 Å passband are available. Moreover, the sensitivity of the IRIS far-ultraviolet SJI detector has been found to decrease significantly in the past two years. The observations used here, taken in January and February 2014, are therefore best suited for a comparative study of the very narrow network jets.

2.2. Unsharp Masking

As mentioned earlier, because grain-like structures and background network emission evolve quickly, the visibility of the network jets is obstructed to a considerable amount. In addition, the jets mostly appear very close to each other in space. They are also observed to recur at the same locations very often in the whole image sequences. It is therefore somewhat difficult

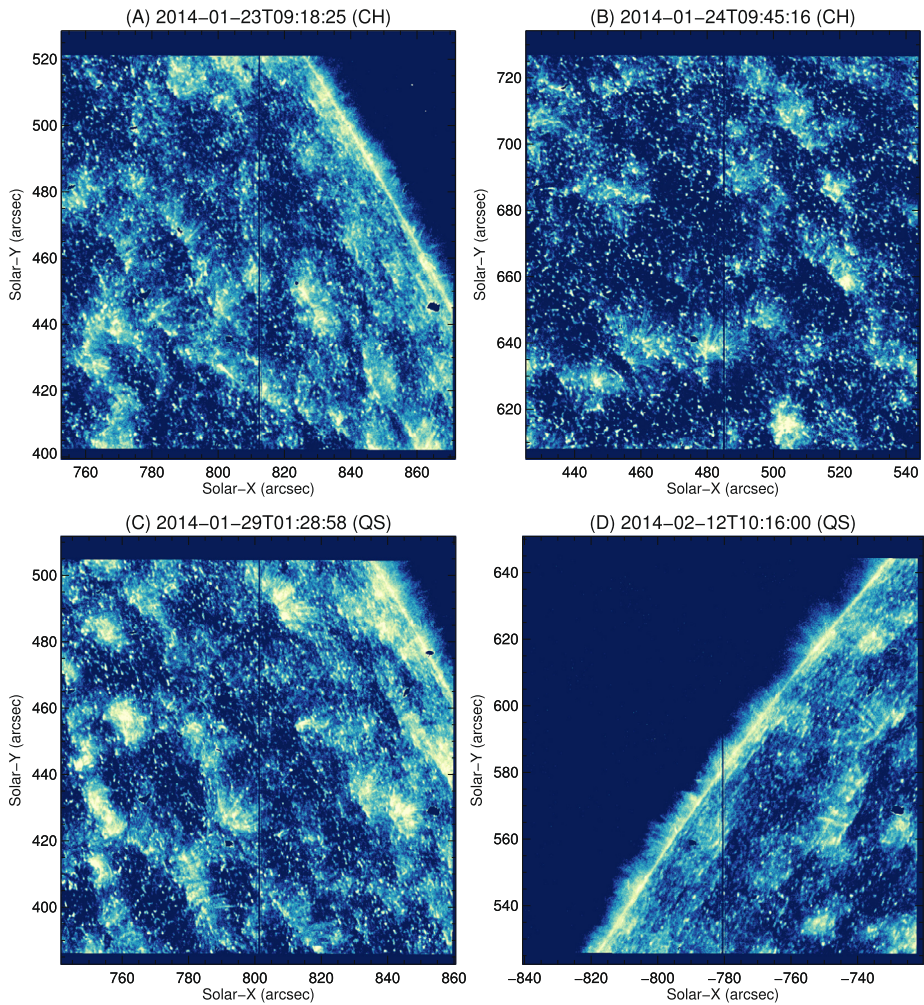


Figure 2 One of the unsharp-masked SJIs in the image sequence of each data-set we used (see Table 1 and Figure 1). A full-FOV movie of the whole image sequence of the original and processed images of data-set (A) can be accessed in the online journal. See also the supplementary materials of the article for the small FOV movies (zoomed) of the datasets B and C, which show the dynamics of the jets more clearly.

to isolate individual jets in SJIs. To enhance the jet structures in the images, we applied the unsharp-masking technique to the SJIs. The technique is explained as follows: For every image in the sequence, a $1'' \times 1''$ (6×6 pixels) box-car-smoothed version of that image is subtracted from the original image. This residual is then added back to the original image. The resulting image is referred to as an unsharp-masked image. This technique was also applied by Tian *et al.* (2014) to enhance the fine features. Figure 2 shows snapshots of the unsharp-masked images in the four observations. We note that as a result of the similar spatial and temporal scales, the bright grain-like features are still present in the unsharp-masked images.

2.3. Space–Time Plots

The technique of space–time (S–T) plots is widely used to derive the apparent speeds of moving features. The observed regions are large, and we can therefore identify many network jets in each of the observations shown in Figure 2. It should be noted that all four observed regions are close to the limb, and the line of sight component of the jet velocities is therefore expected to be small. Hence, the value of apparent speeds derived from S–T plots must be close to the real velocities of the jets.

We visually identified 31 jets in dataset A, 36 in B (making a total of 67 jets in CHs), 52 jets in dataset C, and 8 in D (which is a total of 60 jets in QS regions). They show relatively strong emission in the 1330 Å image sequences. The jets were selected such that every jet was well isolated from others in space and time. We were careful to ensure that the selected jets are less affected by the bright grain-like structures and thus showed clear signatures in the S–T plots. It is important to emphasize here that we were only able to measure the relatively strong jets, which are only small fraction (roughly $\sim 20\text{--}30\%$) of the network jets present in the data. We also note that dataset D has only eight jets that can be reliably traced because this dataset is shorter (see Table 1) and, most important, there is more off-limb region in the field of view than in other datasets (see Figure 2 (D)).

For each identified jet, we first drew a line (curved or straight) along the direction of the jet propagation (see example in Figure 3 (A) and (C)). The intensity along this line was plotted and

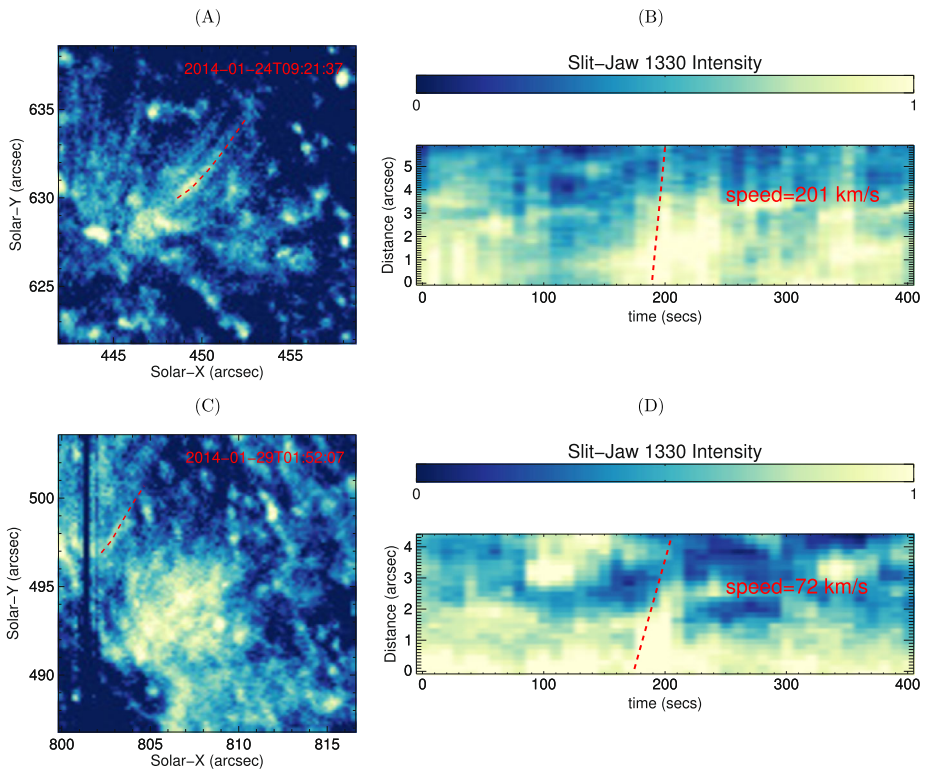


Figure 3 (A) A small FOV of one of the unsharp-masked images of dataset B (see Figure 2). The dashed line indicates the path of a jet. (B) S–T map for the jet marked in (A). (C) Same as (A), but for dataset C. (D) S–T map for the jet marked in (C).

then stacked with time (Figure 3 (B) and (D)). The lifetime and maximum length of the jet can be obtained directly from the S–T map. The measurements made here are solely based on visual inspection. The weak emission of the jets and complications by the network grains made it very difficult to use an automatic method. The shortest observed lifetime is 20 s, although it may be possible that many jets have lifetimes shorter than 20 s because the observations are limited by a cadence of 10 s. The apparent speed can be calculated as the slope of the inclined strip in the S–T plot. For example, the apparent speed of the jet marked in Figure 3 (A) and (B) was calculated to be 201 km s^{-1} and that in Figure 3 (C) and (D) was calculated to be 72 km s^{-1} . All four datasets were analyzed independently by the first two authors. The results they obtained are generally consistent. It is important to note that the uncertainty in the speed measurement is dictated by the spatial resolution and time cadence of the data. The spatial resolution of IRIS SJIs is $\sim 250 \text{ km}$, and the cadence of all the datasets is 10 s, which means that the smallest uncertainty in the jet speed calculation is $\sim 25 \text{ km s}^{-1}$.

2.4. Footpoint Brightness

We mentioned in Section 1 that the network jets are mostly preceded by footpoint brightenings. It is important to explore the effect of local heating on the dynamical properties of the jets, therefore we calculated the increase in footpoint brightness for every jet. The footpoint of a jet is defined as the location of origin of the jet. We chose a 2×2 pixel area around the footpoint of the jet. The intensity within this area was determined at the instant that is closest to the appearance of the jet, when the brightness at the foot-point is highest, which we call *brightness*. The intensity at the same location was determined in two more frames in the image sequence, one before and one after the frame of highest intensity at the footpoint. These two frames were selected such that there was no enhanced brightening at the location of the jet footpoint compared to the surrounding area. The average intensities at the footpoint location of these two frames was calculated, which we call *average*. This *average* was subtracted from the *brightness* (as termed above). The result was divided by the *average* and multiplied by 100 to derive the percentage. Please note that when we write “intensity”, we mean throughout the total data counts in the 2×2 pixel area obtained from the original SJIs.

3. Results and Discussion

We analyzed different properties of the network jets (mainly apparent speed, length, lifetime, and increase in footpoint brightness) to study their dynamics and to compare CH and QS region jets. The comparison clearly shows that the average values of the apparent speed and length of jets in CHs are significantly greater than those in QS regions, as shown in Figure 4. The QS region results are marked in red, the CH results are represented by blue histograms. However, no such demarcation exists for lifetimes and footpoint brightness increase. The comparison of the calculated average values (with standard deviation) of these properties is summarized in Table 2.

Table 2 Average properties of network jets. The errors are standard deviations of the respective distribution.

	Coronal hole	Quiet Sun
Speed (km s^{-1})	186 ± 62	109 ± 39
Length (Mm)	4.9 ± 1.7	3.5 ± 1.2
Lifetime (s)	27 ± 6	33 ± 8
FP brightness increase (%)	36 ± 31	36 ± 26

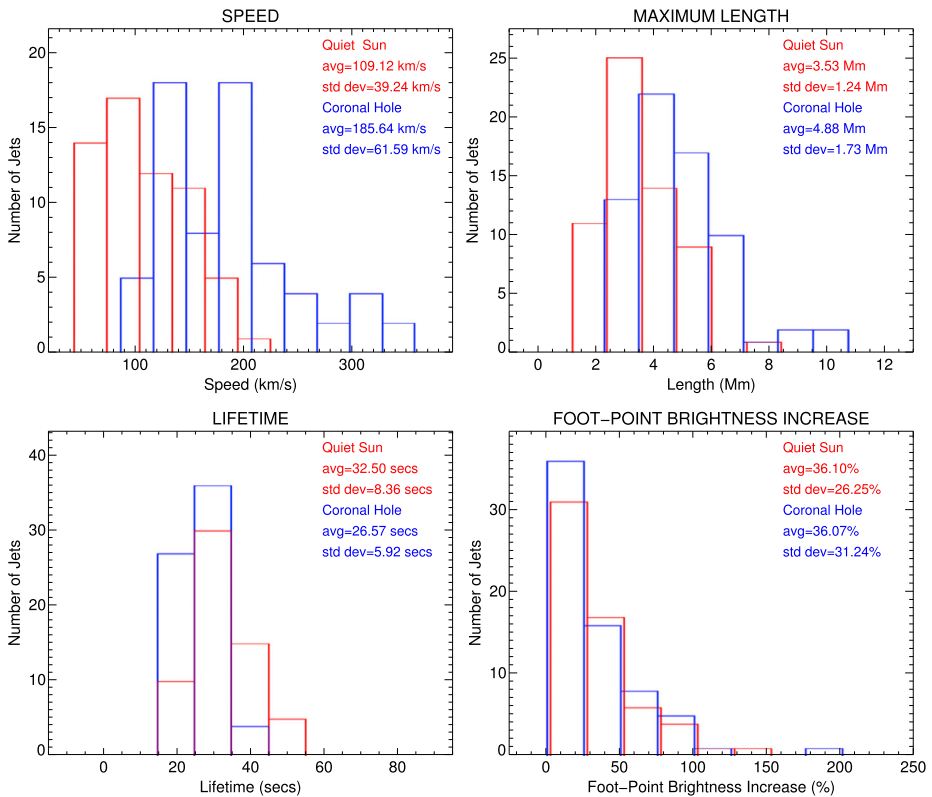


Figure 4 Distribution of different parameters of network jets showing comparison between CH and QS regions. The total sample number for CH distributions (indicated by blue color) is 67 jets and that for QS region distributions (indicated by red color) is 60 jets.

CH jets appear to be faster and longer than QS region jets, which may be a consequence of different magnetic configurations in the CH and QS areas. In CHs, open and expanding magnetic flux tubes at network boundaries must be assisting the small-scale network jets in propagating up to larger extents with higher speeds, and the jets are therefore accelerated more efficiently in CHs than in QS regions. This result is consistent with a recent numerical simulation of chromospheric jets by Iijima and Yokoyama (2015). These authors pointed out that these jets are projected farther outward with higher speeds when overlying coronal gas pressure is lower (similar to that in a coronal hole). On the other hand, the jets propagate up to a shorter distance when the coronal gas pressure is higher (similar to that in the quiet Sun), which agrees with our observations. The authors explained that in their simulation the jets are generated by chromospheric shocks, and the amplification of a chromospheric shock wave will be different in CH and QS regions. That we observed greater apparent speeds of these jets in CHs than in the QS regions also allows exploring the suggestions made by Tian *et al.* (2014) and Rouppe van der Voort *et al.* (2015), that some network jets might be TR manifestations of rapid blueward excursions (RBEs). It has already been claimed (*e.g.* Rouppe van der Voort *et al.*, 2009, Sekse, Rouppe van der Voort, and De Pontieu, 2012, Pereira *et al.*, 2014) that the RBEs observed in profiles of different chromospheric lines are on-disk counterparts of solar spicules. In addition, it is also reported that the Doppler velocity of RBEs increases along their length in CHs when observed in the 8542 Å (Ca II) spectral line using the *CRisp Imaging SpectroPolarimeter instrument* (CRISP, Scharmer *et al.*, 2008) at the

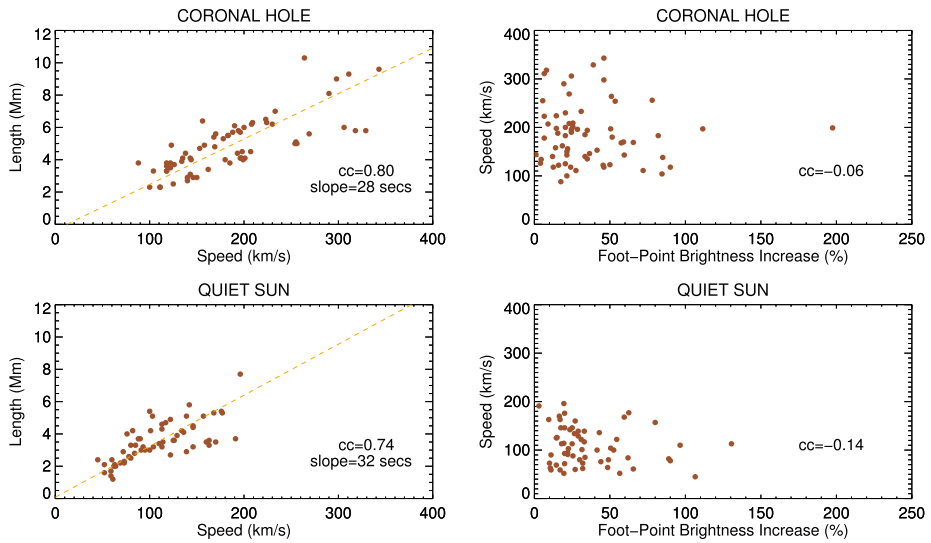


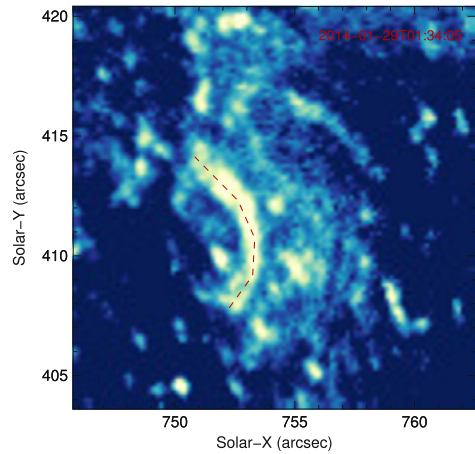
Figure 5 Scatter plots for different parameters of network jets. The correlation coefficients (cc) are indicated.

Swedish 1-m Solar Telescope (SST). However, no such trend was observed for QS region RBEs (see Sekse *et al.*, 2013 for detailed discussion). This correspondence between the increasing trend in the Doppler velocity of RBEs (observed in the chromosphere) and higher speeds of the network jets (observed in the TR) in CHs provide more evidence that the RBEs, or on-disk spicules, may be the signatures of parts or phases of the network jets that have lower temperature and are less accelerated.

The distribution and average value of the footpoint brightness increase is almost the same in CH and QS regions. The similar magnitude suggests that the same generation mechanism of the network jets is at work in both regions. In addition, we studied the interrelation of the jet properties in respective regions in Figure 5. We find that the apparent speed of the network jets is independent of the increase in footpoint brightness, although it is very much dependent on length of the jets. As indicated in Figure 5, speed and length of the jets are highly correlated in both CH and QS regions with a correlation coefficient of 0.80 for CH and 0.74 for QS region jets. On the other hand, the brightness increase at the footpoints appears to be independent of any of the dynamical properties of the jets. This again reflects that the basic mechanism (*e.g.* magnetic reconnection) responsible for the generation of the network jets is of very similar nature in CH and QS regions. However, as the jets propagate in different ambient magnetic environments in the two regions, most of the dynamical properties are considerably affected.

The recurrence of these high-speed network jets from the same location suggests that the oscillatory reconnection might be a possible mechanism for the generation of the jets. It has already been demonstrated by Murray, van Driel-Gesztelyi, and Baker (2009) and McLaughlin *et al.* (2012) that such a reconnection can trigger quasi-periodic upflows. It is also reported that models driven by the Lorentz force are able to produce heat and accelerate spicules (Martínez-Sykora, Hansteen, and Moreno-Insertis, 2011; Goodman, 2014). The recent numerical simulation by Goodman (2014) even claims that jets driven by the Lorentz force can have speeds as high as $66\text{--}397\text{ km s}^{-1}$, similar to speeds we found here. However, the pressure-driven jets (*e.g.* Martínez-Sykora, Hansteen, and Moreno-Insertis, 2011; Judge *et al.*, 2012) are reported to only gain speeds of $\sim 60\text{ km s}^{-1}$. Based on the above-mentioned numerical simulation results along with our observations, it can therefore be concluded that the evolution of the magnetic field at small scales has a key role in the generation and acceleration of high-speed jets in the chromo-

Figure 6 One example of a compact bright loop observed in QS regions. The red dashed curve indicates the loop-like feature.



sphere and TR. It is important to note that the optically thin Si IV lines do not have a high enough signal-to-noise ratio in the 4 s exposure data, which means that the spectral data cannot be used in these observations. Without a detailed analysis of the spectroscopic data, we cannot exclude the possibility that some of the apparent motions may be a reflection of the ionization front or even shock waves and may not be real mass flows (see Tian *et al.*, 2014 for a detailed discussion).

We have already indicated that the mechanism generating the network jets is probably similar in the CH and QS regions. If the generation mechanism is magnetic reconnection in the chromosphere (e.g. Shibata *et al.*, 2007, Yurchyshyn, Abramenko, and Goode, 2013, Deng *et al.*, 2015, Ni *et al.*, 2015), it would indicate that there is no significant difference of magnetic structures in the chromospheric layers of CH and QS regions. In CHs, the mechanism is probably the reconnection of small chromospheric loops with the open flux in the network. Whereas in the QS regions, small chromospheric loops may reconnect with the legs of the coronal loops. Higher up in the TR and corona, there are probably not many loops in the CH, while in QS regions many TR and coronal loops are still present. Our observations provide direct-imaging evidence to validate this proposed idea because we have found some small compact loop-like bright features to be present in QS regions (probably the TR loops reported by Hansteen *et al.*, 2014). An example of such a loop detected in our observations in QS regions is shown in Figure 6. These bright loop-like regions have typical extents of $\sim 5''$ and are generally devoid of the network jets. In CH, no such features can be observed, which suggests that at the layers of TR in a CH, there are basically only open field lines and almost no loops. This result is also consistent with the findings of Wiegelmann and Solanki (2004) and Tian *et al.* (2008b) that loops reside only at very low layers in a CH. The difference in magnetic morphology in higher layers is most likely responsible for the different propagation of the network jets in the two regions, leading to higher speed and longer distance in CHs. That the observed QS region compact loops are generally devoid of network jets suggests that the network jets occurred below the height of these TR loops, which means that the network jets are probably produced in the chromosphere.

In addition to explanations involving magnetic reconnection, some other models may be able to account for the observed properties of the jets. Hollweg, Jackson, and Galloway (1982) proposed that magneto-hydrodynamic waves could exert a time-averaged upward nonthermal pressure and thus “levitate” the cool chromosphere. This was suggested as a formation mechanism for large type I solar spicules (see also De Pontieu, 1999, Kudoh and Shibata, 1999, Matsumoto and Shibata, 2010). Cranmer and Woolsey (2015) recently extended this idea to smaller-scale turbulent Alfvénic motions in CH network regions and found that nonlinear mode conversion into chromospheric shocks may provide intermittent upflows of the necessary order of magni-

tude. Such a model produces vertical excursions in the height of the transition region of about 1 to 6 Mm over timescales of 20 to 60 s, which gives rise to apparent jet-like velocities of 50 to 200 km s⁻¹. The wave or turbulence model for jet formation is observationally distinguishable from a reconnection-based model in that the former does not require a magnetic field of both polarities to be present at the jet footpoint location.

The prevalence of the network jets and that the jets reach higher layers (~ 5 Mm) in both regions (CH and QS regions) implies that they may play an important role in supplying mass and energy to the corona and solar wind. At this stage, we must reconcile the implications on the origin of the solar wind (Tian *et al.*, 2014) that arises from these intermittent small-scale network jets in the TR. However, IRIS observations are unable to detect heating signatures of these network jets at coronal temperatures because IRIS is designed to study mainly the chromosphere and TR. At its spectral coverage only one line is present, Fe XII 1349 Å, which is formed at normal coronal temperatures but it is usually very weak or absent. The observations show only that the jets reach at least ~ 10⁵ K, but at present we cannot determine whether they can be heated to coronal temperatures. In the near future, we will try to track these jets to coronal structures. One way, for instance, would be to investigate the possible connection between these jets and the hot intermittent upflows along plume-like structures (McIntosh *et al.*, 2010; Tian *et al.*, 2011; Pucci *et al.*, 2014; Pant *et al.*, 2015) and the blue-shift patches of lower-coronal lines (Tian *et al.*, 2008a, 2009; Fu *et al.*, 2014). Moreover, we must also try to address the question of energy dissipation by the network jets in the corona, *e.g.*, whether they trigger compressional waves (Gupta *et al.*, 2012; Uritsky *et al.*, 2013; Jiao *et al.*, 2015; Pant *et al.*, 2015). This aspect can be studied in more detail to further explore the difference in mechanisms between CH and QS regions in generating network jets and in processing the supplied mass and energy by these jets to the corona and solar wind. In this context, new instruments with similar spatial and spectral resolution as that of IRIS, along with wider wavelength coverage, can provide cospatial and cotemporal observations of the TR and corona, are also desirable. For instance, the *Extreme Ultraviolet Imager* (EUI) and *Spectral Imaging of the Coronal Environment* (SPICE) instruments onboard the *Solar Orbiter* spacecraft (Müller *et al.*, 2013), to be launched in October 2018, can provide more insight into the heating process of the network jets. This will serve as a great opportunity for a better understanding of the relation between the TR network jets and coronal structures and outflows.

4. Summary

Our IRIS observations revealed network jets in QS regions along with earlier detections in CHs. We comparatively analyzed CH and QS regions based on the properties of these jets. It must be noted that the results obtained are limited by the number of datasets used for the study. We used only two observations in CH and two in QS regions. Hence, we cannot conclude if the results will change by using more observations. Our results from the current study are summarized as follows:

1. CH jets appear to be faster and longer than those in QS regions. This is most likely a consequence of the different magnetic configurations of the two regions, with open magnetic field lines dominant in CH and magnetic loops often present in QS regions. This proposed idea is well supported by our observations, which clearly show some compact bright loops to be present in QS regions, but they are generally absent in CH at TR heights.
2. Recently, RBEs have been reported to show an increasing trend in the Doppler velocity along their length in CH. The higher apparent speed of network jets in CH can provide evidence to support the proposed idea that TR network jets are the accelerated phase of RBEs in coronal holes.
3. The similar distribution and average value of the increase in footpoint brightness indicates that the same generation mechanism is at work in these jets in both regions. Moreover, we

found a good correlation between the apparent speed and length of the jets. On the other hand, the footpoint brightness increase seems to be independent of any of the dynamical properties of the jets.

4. As these jets reach higher layers (length of ~ 5 Mm), they can serve as reasonable candidates for supplying mass and energy to the corona and solar wind. However, it is important to note that IRIS observations are unable to detect the signatures of these jets beyond $\sim 10^5$ K.

Acknowledgements We would like to thank the anonymous referee for the constructive comments that have enabled us to improve the manuscript. The authors are grateful to the IRIS team for making the data publicly available. IRIS is a NASA Small Explorer mission developed and operated by the Lockheed Martin Solar and Astrophysics Laboratory (LMSAL), with mission operations executed at the NASA Ames Research Center and major contributions to downlink communications funded by the Norwegian Space Center (Norway) through a European Space Agency PRODEX contract. This work was supported by contract 8100002705 from LMSAL to SAO and the NSF REU solar physics program at SAO, grant number AGS-1263241. N.N. would like to thank the Human Resource Development Group (HRDG) of the Council of Scientific and Industrial Research (CSIR), India for a Junior Research Fellowship (JRF) award. H.T. is supported by the Recruitment Program of Global Experts of China and NSFC under grant 41574166. We would like to thank Haruhisa Iijima for valuable suggestions.

References

- Axford, W.I., McKenzie, J.F.: 1992, In: Marsch, E., Schwenn, R. (eds.) *Solar Wind Seven Colloquium*, 1. [ADS](#).
- Carlsson, M., Stein, R.F.: 1997, *Astrophys. J.* **481**, 500. [ADS](#).
- Cranmer, S.R.: 2009, *Living Rev. Solar Phys.* **6**, 3. [DOI](#). [ADS](#).
- Cranmer, S.R., Woolsey, L.N.: 2015, *Astrophys. J.* **812**, 71. [DOI](#). [ADS](#).
- De Pontieu, B.: 1999, *Astron. Astrophys.* **347**, 696. [ADS](#).
- De Pontieu, B., Rouppe van der Voort, L., McIntosh, S.W., Pereira, T.M.D., Carlsson, M., Hansteen, V., Skogsrud, H., Lemen, J., Title, A., Boerner, P., Hurlburt, N., Tarbell, T.D., Wuelser, J.P., De Luca, E.E., Golub, L., McKillop, S., Reeves, K., Saar, S., Testa, P., Tian, H., Kankelborg, C., Jaeggli, S., Kleint, L., Martínez-Sykora, J.: 2014a, *Science* **346**, 1255732. [DOI](#). [ADS](#).
- De Pontieu, B., Title, A.M., Lemen, J.R., Kushner, G.D., Akin, D.J., Allard, B., Berger, T., Boerner, P., Cheung, M., Chou, C., Drake, J.F., Duncan, D.W., Freeland, S., Heyman, G.F., Hoffman, C., Hurlburt, N.E., Lindgren, R.W., Mathur, D., Rehse, R., Sabolish, D., Seguin, R., Schrijver, C.J., Tarbell, T.D., Wülser, J.-P., Wolfson, C.J., Yanari, C., Mudge, J., Nguyen-Phuc, N., Timmons, R., van Bezooijen, R., Weingrod, I., Brookner, R., Butcher, G., Dougherty, B., Eder, J., Knagenhjelm, V., Larsen, S., Mansir, D., Phan, L., Boyle, P., Cheimets, P.N., DeLuca, E.E., Golub, L., Gates, R., Hertz, E., McKillop, S., Park, S., Perry, T., Podgorski, W.A., Reeves, K., Saar, S., Testa, P., Tian, H., Weber, M., Dunn, C., Eccles, S., Jaeggli, S.A., Kankelborg, C.C., Mashburn, K., Pust, N., Springer, L., Carvalho, R., Kleint, L., Marmie, J., Mazmanian, E., Pereira, T.M.D., Sawyer, S., Strong, J., Worden, S.P., Carlsson, M., Hansteen, V.H., Leenaarts, J., Wiesmann, M., Aloise, J., Chu, K.-C., Bush, R.I., Scherrer, P.H., Brekke, P., Martínez-Sykora, J., Lites, B.W., McIntosh, S.W., Uitenbroek, H., Okamoto, T.J., Gummin, M.A., Auker, G., Jerram, P., Pool, P., Waltham, N.: 2014b, *Solar Phys.* **289**, 2733. [DOI](#). [ADS](#).
- Deng, N., Chen, X., Liu, C., Jing, J., Tritschler, A., Reardon, K.P., Lamb, D.A., Deforest, C.E., Denker, C., Wang, S., Liu, R., Wang, H.: 2015, *Astrophys. J.* **799**, 219. [DOI](#). [ADS](#).
- Fu, H., Xia, L., Li, B., Huang, Z., Jiao, F., Mou, C.: 2014, *Astrophys. J.* **794**, 109. [DOI](#). [ADS](#).
- Goodman, M.L.: 2014, *Astrophys. J.* **785**, 87. [DOI](#). [ADS](#).
- Gupta, G.R., Teriaca, L., Marsch, E., Solanki, S.K., Banerjee, D.: 2012, *Astron. Astrophys.* **546**, A93. [DOI](#). [ADS](#).
- Habbal, S.R., Woo, R., Arnaud, J.: 2001, *Astrophys. J.* **558**, 852. [DOI](#). [ADS](#).
- Hansteen, V.H., Velli, M.: 2012, *Space Sci. Rev.* **172**, 89. [DOI](#). [ADS](#).
- Hansteen, V., De Pontieu, B., Carlsson, M., Lemen, J., Title, A., Boerner, P., Hurlburt, N., Tarbell, T.D., Wuelser, J.P., Pereira, T.M.D., De Luca, E.E., Golub, L., McKillop, S., Reeves, K., Saar, S., Testa, P., Tian, H., Kankelborg, C., Jaeggli, S., Kleint, L., Martínez-Sykora, J.: 2014, *Science* **346**, 1255757. [DOI](#). [ADS](#).
- He, J.-S., Tu, C.-Y., Marsch, E.: 2007, *Astron. Astrophys.* **468**, 307. [DOI](#). [ADS](#).
- Hollweg, J.V., Jackson, S., Galloway, D.: 1982, *Solar Phys.* **75**, 35. [DOI](#). [ADS](#).
- Iijima, H., Yokoyama, T.: 2015, *Astrophys. J.* **812**, L30. [DOI](#). [ADS](#).

- Jiao, F., Xia, L., Li, B., Huang, Z., Li, X., Chandrashekhara, K., Mou, C., Fu, H.: 2015, *Astrophys. J. Lett.* **809**, L17. DOI. ADS.
- Judge, P.G., De Pontieu, B., McIntosh, S.W., Olluri, K.: 2012, *Astrophys. J.* **746**, 158. DOI. ADS.
- Kudoh, T., Shibata, K.: 1999, *Astrophys. J.* **514**, 493. DOI. ADS.
- Lemen, J.R., Title, A.M., Akin, D.J., Boerner, P.F., Chou, C., Drake, J.F., Duncan, D.W., Edwards, C.G., Friedlaender, F.M., Heyman, G.F., Hurlburt, N.E., Katz, N.L., Kushner, G.D., Levay, M., Lindgren, R.W., Mathur, D.P., McFeaters, E.L., Mitchell, S., Rehse, R.A., Schrijver, C.J., Springer, L.A., Stern, R.A., Tarbell, T.D., Wuelser, J.-P., Wolfson, C.J., Yanari, C., Bookbinder, J.A., Cheimets, P.N., Caldwell, D., Deluca, E.E., Gates, R., Golub, L., Park, S., Podgorski, W.A., Bush, R.I., Scherrer, P.H., Gumm, M.A., Smith, P., Auker, G., Jerram, P., Pool, P., Soufli, R., Windt, D.L., Beardsley, S., Clapp, M., Lang, J., Waltham, N.: 2012, *Solar Phys.* **275**, 17. DOI. ADS.
- Martínez-Sykora, J., Hansteen, V., Moreno-Insertis, F.: 2011, *Astrophys. J.* **736**, 9. DOI. ADS.
- Martínez-Sykora, J., Rouppe van der Voort, L., Carlsson, M., De Pontieu, B., Pereira, T.M.D., Boerner, P., Hurlburt, N., Kleint, L., Lemen, J., Tarbell, T.D., Title, A., Wuelser, J.-P., Hansteen, V.H., Golub, L., McKillop, S., Reeves, K.K., Saar, S., Testa, P., Tian, H., Jaeggli, S., Kankelborg, C.: 2015, *Astrophys. J.* **803**, 44. DOI. ADS.
- Matsumoto, T., Shibata, K.: 2010, *Astrophys. J.* **710**, 1857. DOI. ADS.
- McIntosh, S.W., Innes, D.E., De Pontieu, B., Leamon, R.J.: 2010, *Astron. Astrophys.* **510**, L2. DOI. ADS.
- McLaughlin, J.A., Verth, G., Fedun, V., Erdélyi, R.: 2012, *Astrophys. J.* **749**, 30. DOI. ADS.
- Müller, D., Marsden, R.G., St. Cyr, O.C., Gilbert, H.R.: 2013, *Solar Phys.* **285**, 25. DOI. ADS.
- Murray, M.J., van Driel-Gesztelyi, L., Baker, D.: 2009, *Astron. Astrophys.* **494**, 329. DOI. ADS.
- Ni, L., Kliem, B., Lin, J., Wu, N.: 2015, *Astrophys. J.* **799**, 79. DOI. ADS.
- Pant, V., Dolla, L., Mazumder, R., Banerjee, D., Krishna Prasad, S., Panditi, V.: 2015, *Astrophys. J.* **807**, 71. DOI. ADS.
- Pereira, T.M.D., De Pontieu, B., Carlsson, M., Hansteen, V., Tarbell, T.D., Lemen, J., Title, A., Boerner, P., Hurlburt, N., Wülsel, J.P., Martínez-Sykora, J., Kleint, L., Golub, L., McKillop, S., Reeves, K.K., Saar, S., Testa, P., Tian, H., Jaeggli, S., Kankelborg, C.: 2014, *Astrophys. J. Lett.* **792**, L15. DOI. ADS.
- Pucci, S., Poletto, G., Sterling, A.C., Romoli, M.: 2014, *Astrophys. J.* **793**, 86. DOI. ADS.
- Rouppe van der Voort, L., Leenaarts, J., De Pontieu, B., Carlsson, M., Vissers, G.: 2009, *Astrophys. J.* **705**, 272. DOI. ADS.
- Rouppe van der Voort, L., De Pontieu, B., Pereira, T.M.D., Carlsson, M., Hansteen, V.: 2015, *Astrophys. J. Lett.* **799**, L3. DOI. ADS.
- Rutten, R.J., De Pontieu, B., Lites, B.: 1999, In: Rimmele, T.R., Balasubramaniam, K.S., Radick, R.R. (eds.) *High Resolution Solar Physics: Theory, Observations, and Techniques*, *Astron. Soc. Pac. Conf. Ser.* **183**, 383. ADS.
- Scharmer, G.B., Narayan, G., Hillberg, T., de la Cruz Rodríguez, J., Löfdahl, M.G., Kiselman, D., Sütterlin, P., van Noort, M., Lagg, A.: 2008, *Astrophys. J. Lett.* **689**, L69. DOI. ADS.
- Sekse, D.H., Rouppe van der Voort, L., De Pontieu, B.: 2012, *Astrophys. J.* **752**, 108. DOI. ADS.
- Sekse, D.H., Rouppe van der Voort, L., De Pontieu, B., Scullion, E.: 2013, *Astrophys. J.* **769**, 44. DOI. ADS.
- Shibata, K., Nakamura, T., Matsumoto, T., Otsuji, K., Okamoto, T.J., Nishizuka, N., Kawate, T., Watanabe, H., Nagata, S., UeNo, S., Kitai, R., Nozawa, S., Tsuneta, S., Suematsu, Y., Ichimoto, K., Shimizu, T., Katsukawa, Y., Tarbell, T.D., Berger, T.E., Lites, B.W., Shine, R.A., Title, A.M.: 2007, *Science* **318**, 1591. DOI. ADS.
- Skogsrud, H., Rouppe van der Voort, L., De Pontieu, B., Pereira, T.M.D.: 2015, *Astrophys. J.* **806**, 170. DOI. ADS.
- Tian, H., Tu, C.-Y., Marsch, E., He, J.-S., Zhou, G.-Q.: 2008a, *Astron. Astrophys.* **478**, 915. DOI. ADS.
- Tian, H., Marsch, E., Tu, C.-Y., Xia, L.-D., He, J.-S.: 2008b, *Astron. Astrophys.* **482**, 267. DOI. ADS.
- Tian, H., Marsch, E., Curdt, W., He, J.: 2009, *Astrophys. J.* **704**, 883. DOI. ADS.
- Tian, H., McIntosh, S.W., Habbal, S.R., He, J.: 2011, *Astrophys. J.* **736**, 130. DOI. ADS.
- Tian, H., DeLuca, E.E., Cranmer, S.R., De Pontieu, B., Peter, H., Martínez-Sykora, J., Golub, L., McKillop, S., Reeves, K.K., Miralles, M.P., McCauley, P., Saar, S., Testa, P., Weber, M., Murphy, N., Lemen, J., Title, A., Boerner, P., Hurlburt, N., Tarbell, T.D., Wuelser, J.P., Kleint, L., Kankelborg, C., Jaeggli, S., Carlsson, M., Hansteen, V., McIntosh, S.W.: 2014, *Science* **346**, 1255711. DOI. ADS.
- Tu, C.-Y., Zhou, C., Marsch, E., Xia, L.-D., Zhao, L., Wang, J.-X., Wilhelm, K.: 2005, *Science* **308**, 519. DOI. ADS.
- Uritsky, V.M., Davila, J.M., Viall, N.M., Ofman, L.: 2013, *Astrophys. J.* **778**, 26. DOI. ADS.
- Waldmeier, M.: 1956, *Z. Astrophys.* **38**, 219. ADS.
- Wang, X., McIntosh, S.W., Curdt, W., Tian, H., Peter, H., Xia, L.-D.: 2013, *Astron. Astrophys.* **557**, A126. DOI. ADS.
- Wiegelmann, T., Solanki, S.K.: 2004, *Solar Phys.* **225**, 227. DOI. ADS.

- Wilhelm, K., Curdt, W., Marsch, E., Schühle, U., Lemaire, P., Gabriel, A., Vial, J.-C., Grewing, M., Huber, M.C.E., Jordan, S.D., Poland, A.I., Thomas, R.J., Kühne, M., Timothy, J.G., Hassler, D.M., Siegmund, O.H.W.: 1995, *Solar Phys.* **162**, 189. [DOI](#). [ADS](#).
- Yang, L., He, J., Peter, H., Tu, C., Chen, W., Zhang, L., Marsch, E., Wang, L., Feng, X., Yan, L.: 2013, *Astrophys. J.* **770**, 6. [DOI](#). [ADS](#).
- Yurchyshyn, V., Abramenko, V., Goode, P.: 2013, *Astrophys. J.* **767**, 17. [DOI](#). [ADS](#).